THE ASTROPHYSICAL JOURNAL, 272:665–677, 1983 September 15

OUTER ATMOSPHERES OF COOL STARS. XIV. A MODEL FOR THE CHROMOSPHERE AND TRANSITION REGION OF BETA CETI (G9.5 III)

KJELL ERIKSSON,[1] JEFFREY L. LINSKY,[2,3] and Theodore Simon[4]
Joint Institute for Laboratory Astrophysics, University of Colorado and National Bureau of Standards
Received 1982 December 13; accepted 1983 March 8

ABSTRACT

We compute a model for the chromosphere and transition region of β Ceti (G9.5 III) consistent with *IUE* spectra of the resonance lines of Mg II, C II, and C IV. We treat the Mg II *h* and *k* lines in partial redistribution and the C II and C IV lines in complete redistribution. A good match to the observed line profile fluxes and to the Mg II *k* line profile is achieved for a hydrostatic equilibrium one-component model with temperature plateaus at 5500 K and 22,500 K, but this model is not unique. We present computed line fluxes for a range of models to show the range of permitted temperature structures. Beta Ceti lies immediately to the left of the boundary in the H-R diagram generally separating stars with and without high temperature plasmas. Comparing the β Ceti model to models previously computed in a similar way for other stars, we find a trend of decreasing chromospheric pressures and increasing geometric scales as single stars evolve across the transition region boundary. Also this analysis suggests that the transition region pressures decrease drastically and geometric scales increase rapidly as single giant stars evolve to the right toward the boundary. Beta Ceti is a very luminous X-ray emitter for its spectral type and rotational velocity. Its X-ray brightness could be explained either by a corona containing many high-pressure loops or a high-pressure homogeneous corona overlying an inhomogeneous transition region. The question of pressure balance between the corona and transition region including magnetic forces requires further study.

Subject headings: stars: chromospheres—stars: coronae — stars: individual — stars: late-type — ultraviolet: spectra—X-rays: sources

I. INTRODUCTION

In previous papers (Ayres and Linsky 1975; Kelch *et al.* 1978; Basri, Linsky, and Eriksson 1981), we have computed semiempirical chromospheric models for late-type giants and supergiants by matching computed and observed profiles of the Ca II and Mg II resonance lines using partial redistribution (PRD) diagnostics. These studies have concentrated on the giants β Gem (K0 III), α Boo (K1 + IIIb), and α Tau (K5 III), and the supergiants β Dra (G2 Ib-IIa), ε Gem (G8 Ib), and α Ori (M2 Ia-Iab). The purpose of these investigations, as well as our studies of dwarfs and close binary systems (cf. review by Linsky 1980), is to investigate trends in chromospheric models with stellar effective temperature, gravity, and other properties, and to provide models useful in estimating the chromospheric energy balance for comparison with theoretical models (e.g., review by Ulmschneider 1979; Stein 1981). It is important to recognize that these models are only first-order approximations because they ignore atmospheric extension, which is important in the supergiants (e.g., Bernat *et al.* 1978; Stencel *et al.* 1981), and inhomogeneities such as plage regions. They also are primarily for the chromospheric layers, whereas information on the hotter layers in stellar transition regions is now available from the *International Ultraviolet Explorer* (*IUE*) satellite.

In the present paper we extend our previous work by computing a semiempirical model for the chromosphere and transition region of β Ceti (G9.5 III). We have chosen this star for analysis because it lies at a critical position in the H-R diagram.

Near the beginning of *IUE* operations, Linsky and Haisch (1979) noted from ultraviolet spectra of cool giants and supergiants that the warmer stars with color index $V - R < 0.80$ (the yellow giants) show emission lines formed at all temperatures up to 10^5 K, whereas cooler stars with $V - R > 0.80$ (the red giants) show only chromospheric emission lines. On this basis, they proposed a nearly vertical dividing line in the H-R diagram near $V - R = 0.80$ (see Fig. 1 in Simon, Linsky, and Stencel 1982) separating the yellow giants that

[1]Now at Astromiska Observatoriet, Uppsala, Sweden.
[2]Staff Member, Quantum Physics Division, National Bureau of Standards.
[3]Guest Observer, *International Ultraviolet Explorer*.
[4]Also at the Institute for Astronomy, University of Hawaii.

typically have transition regions (TRs) from the red giants that typically do not. Subsequently, Ayres *et al.* (1981) showed that *Einstein* soft X-ray observations are consistent with the typical presence of hot coronae in single stars to the left of a similar boundary and the absence of coronae in single stars to the right. Also, Stencel (1978) and Stencel and Mullan (1980*a*, *b*) presented evidence for the onset of massive cool winds in stars lying to the right of a similar boundary.

While the idea of a TR boundary has been criticized because of the limited data sample and the existence of a few "hybrid" stars with C IV emission to the right of the proposed boundary, Simon, Linsky, and Stencel (1982) have shown from a much larger sample that this boundary is a real phenomenon, in the sense that single stars to the right of the boundary, with the exception of one hybrid star, contain significantly less 10^5 K plasma than typical single stars to the left of the boundary.

The star β Ceti is of considerable interest because it is one of the coolest single giant stars ($V-R=0.72$) with prominent C IV and X-ray emission. Ayres *et al.* (1981), found that the normalized C IV flux, $f_{\rm C\ IV}/l_{\rm bol}$, is similar to the quiet Sun's but that the normalized X-ray flux, $f_x/l_{\rm bol}$, is about 25 times larger than the quiet Sun's. By contrast, α Boo ($V-R=0.97$), which is the prototypical K giant lying to the right of the boundary, has no detected C IV and X-ray emission, with 3 σ upper limits $f_{\rm C\ IV}/l_{\rm bol} < 0.06\times(f_{\rm C\ IV}/l_{\rm bol})_\odot$ and $f_x/l_{\rm bol} < 0.002\times(f_x/l_{\rm bol})_\odot$ (Ayres, Simon, and Linsky 1982), We also note that β Gem ($V-R=0.75$), for which Kelch *et al.* (1978) computed a chromospheric model, is located close to β Ceti in the H-R diagram yet its normalized X-ray flux, $f_x/l_{\rm bol}$, is only 0.01 that of β Ceti. Thus we believe it is important to compute a model for β Ceti that can be compared with models for less active stars on either side of the boundary as well as active stars in this region of the H-R diagram. In § II we discuss the parameters of this star and the *IUE* observations. We discuss our procedures for computing a model for the chromosphere and transition region of β Ceti in § III, and compare this model to those of other giant stars in § IV. We also discuss the implications of the X-ray data in § IV.

II. STELLAR PARAMETERS AND *IUE* OBSERVATIONS

We list in Table 1 the basic parameters for β Ceti = HR 188 = HD 4128. Since there is no evidence for binarity, we compare β Ceti to β Gem, α Boo, and other single stars located nearby in the H-R diagram. The parallax of β Ceti is well determined as this star is an IAU Standard Star; we can therefore accurately derive its radius from the distance and Barnes-Evans angular diameter. Our choice of surface gravity is based on this radius and a stellar mass of 2.5 $M_\odot$, estimated by interpolation between Iben's (1967) evolutionary tracks on the assumption that the star is ascending the giant branch for the first time. This assumption appears reasonable, given that β Ceti has bright ultraviolet and X-ray emission and thus may not have lost most of its angular momentum due to the action of its stellar wind. Also Zirin (1976) and O'Brien (1980) noted that the He I λ10830 line is stronger and broader than in most G and K giants. Smith and Dominy (1979) measured $v_{\rm rot}\sin i = 3.3\pm0.8$ km s^{-1}, which is not unusually large for their sample of late G to early K giants, but they called attention to the abnormally large macroturbulent velocity (4.2 ± 0.2 km s^{-1}), which could be related to the large ultraviolet emission-line and X-ray fluxes if such motions are dissipated as heat by shocks in the chromosphere and corona.

In a recent paper Gray (1982*a*) has presented new measurements of $v\sin i$, microturbulent, and macroturbulent velocities. These observations again indicate that β Ceti is anomalous. Although most late giant stars show larger macroturbulent velocities derived from weak than from strong lines (i.e., a decrease with height of the motions which contribute to the macroturbulent broadening of spectral lines), Gray derives for β Ceti the same value (4.2 km s^{-1}) for the macroturbulent velocities from both weak and strong lines. The projected rotation, $v\sin i = 3.0$ km s^{-1} (which agrees very well with that of Smith and Dominy), although typical of a late-type giant star, means that β Ceti has an unusually large value of L_x for its measured rotation. For a discussion of the soft X-ray luminosity dependence on rotation, see, e.g., Pallavicini *et al.* (1981). This anomaly could, of course, be easily resolved if β Ceti is viewed nearly pole-on (Gray 1982*b*).

Although β Ceti is commonly classified a K1 III star, its $V-R$ color is very blue for this spectral type. On this basis Ayres, Marstad, and Linsky (1981, hereafter AML) suggested that it is a late G giant. Woods (1956) and Eggen (1956) classified this star as G8 III, and Gray (1982*a*) proposed K0 III. We here adopt Keenan's (1982) classification of G9.5 III CH-1, under the revised MK system. He notes that the star has normal CN band strength but its CH band is definitely weak. The effective temperature and bolometric corrections cited in Table 1 have been obtained from the theoretical calibration by Bell and Gustafsson (1978), based on the observed $V-R$ color.

The ultraviolet observations analyzed in this paper are from two *IUE* spectra: a short-wavelength low-resolution spectrum, SWP 2371, obtained on 1978 August 23 with an exposure time of 40 minutes, and a long-wavelength high-resolution spectrum, LWR 2155, obtained on the same day with an exposure time of 4 minutes. These large aperture spectra are shown in Figures 1 and 2, respectively. They were reduced using an interactive echelle ripple correction algorithm and the corrected SWP intensity transfer function (Holm 1979; see also

TABLE 1

STELLAR PARAMETERS FOR β CETI = HR 188 = HD 4128

Parameter	Comments
Spectral type = G9.5 III, CH-1	Keenan 1982
$V = 2.02$ mag	Johnson *et al.* 1966
$V - R = 0.72$ mag	Johnson *et al.* 1966
$\pi = 61$ milli-arcsec	Hoffleit 1982
$\phi' = 5.03$ milli-arcsec	Stellar angular diameter derived by using the Barnes-Evans relations; see Linsky *et al.* 1979
$d = 16.4$ pc $= 5.1 \times 10^{19}$ cm	
$R_\star = 6.2 \times 10^{11}$ cm $= 8.9\ R_\odot$	
$M_V = 0.95$ mag	Assuming no interstellar extinction
$M_{bol} = 0.69$ mag	Assuming B.C. $= -0.26$, from Bell and Gustafsson 1978
$L_{bol} = 1.6 \times 10^{35}$ ergs s^{-1} $= 42\ L_\odot$	Assuming $M_{bol,\odot} = 4.76$ and $L_\odot = 3.826 \times 10^{33}$ ergs s^{-1}
$l_{bol} = 5.1 \times 10^{-6}$ ergs s^{-1} cm^{-2}	Apparent bolometric luminosity
$f/F = (R_\star/d)^2 = 1.5 \times 10^{-16}$	Ratio of observed flux to stellar surface flux
$T_{eff} = 4900$ K	From Bell and Gustafsson 1978
$\log g = 2.9$	Assuming a stellar mass of 2.5 $M_\odot$, from Iben 1967
[Fe/H] = 0.0	Overall metal content, from Helfer 1969 and Hansen and Kjaergaard 1971

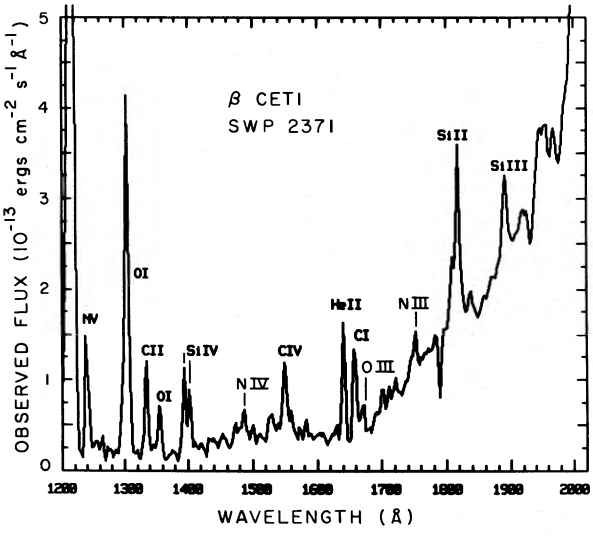

FIG. 1.—A 40 minute large aperture *IUE* spectrum of β Ceti, obtained with the SWP low-dispersion camera. Prominent emission lines and blends are noted.

Cassatella *et al.* 1980); fluxes for several of these features are given by AML.

Table 2 gives the stellar surface fluxes for the most prominent emission features in the 6 Å resolution low-dispersion spectrum. Also given in Table 2 are (f_l/l_{bol}), the fraction of the total stellar luminosity emitted in an emission line, and the ratio of this normalized flux to the same quantity for the Sun (for which the values come mostly from Rottman 1981). These ratios are typically close to unity, but those for N v λ1240 (noted by Linsky and Haisch 1979) and soft X-rays are anomalously large. These latter two ratios, as discussed below, suggest rather large densities for the transition region and corona, perhaps confined by magnetic loops.

III. COMPUTATIONAL PROCEDURES

We have computed model atmospheres that are plane-parallel, laterally homogeneous, and static. The photospheric portions of the models were derived by interpolating in effective temperature between the line-blanketed models given in Bell *et al.* (1976) for $\log g = 3.0$ and solar abundances. The depth variable in the present work is the mass column density, m, or reduced mass column density, m_R; m measures the amount of gas above 1 cm^2 at a given depth; $m_R = m - m_{top}$, where m_{top} is the amount of material lying above the first depth point in the model, usually at $T = 10^5$ K. The location of the temperature minimum was assumed to be $m_{min} = 0.185$, following the scaling law given in Ayres (1979). Our best fit model has $T_{min} = 3575$ K, so that $T_{min}/T_{eff} = 0.73$, a value which is somewhat lower than the relation given in Kelch *et al.* (1978).

Before describing the different procedures used in the computer modeling, we must emphasize that the adopted models are not unique. Some of their specific features are somewhat arbitrary, but this is necessary in order to reduce the number of free parameters (e.g., the value of the TR temperature gradient). It is certainly possible that somewhat different $T(m)$ distributions could fit the available observations equally well or perhaps better, but we postpone to a later time the construction of more definitive models that require high-resolution TR line profile data.

To arrive at a satisfactory model, we performed the following steps iteratively, although we did not go through all steps for each of the assumed $T(m_R)$ and $v_t(m_R)$ distributions (cf. Simon, Kelch, and Linsky 1980).

1. We assumed trial $T(m_R)$ and $v_t(m_R)$ distributions, where v_t is the so-called microturbulent velocity, and adopted a value for m_{top}.

2. We solved the coupled radiative transfer (RT) and statistical equilibrium (SE) system of equations using the complete linearization technique for a hydrogen model atom and assuming hydrostatic equilibrium for the

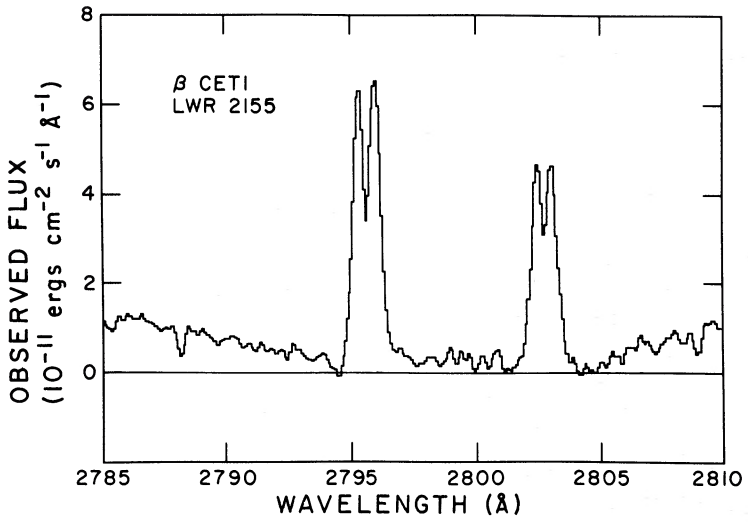

FIG. 2.—A 4 minute large aperture *IUE* spectrum of β Ceti including the Mg II resonance lines, obtained with the LWR high-dispersion camera and reduced with an interactive echelle ripple correction.

TABLE 2

OBSERVED EMISSION LINES AND BLENDS

λ (Å)	Ion	Surface Flux (ergs cm^{-2} s^{-1})	f_l/l_{bol} (10^{-7})	$\frac{(f_l/l_{bol})^a}{(f_l/l_{bol})_\odot}$	References[b]
3–60 ...	Soft X-rays	144,000	40	15.0	2
1176 ...	C III	2,900	0.9	...	1
1240 ...	N V	6,400	1.9	18.0	1, 2
1304 ...	O I	21,000	6.1	6.9	1, 2
1335 ...	C II	3,500	1.0	1.0	1, 2
1356 ...	[O, I]	2,400	0.7	10.0	1
1400 ...	Si IV	5,300	1.6	2.7	1, 2
1526 ...	Si II	1,800:	0.5	3.9	1
1549 ...	C IV	3,600	1.0	1.0	1, 2
1640 ...	He II	3,700	1.1	5.0	1, 2
1657 ...	C I	3,400	1.0	0.7	1
1812 ...	Si II	15,000	4.5	1.2	1, 2
1892 ...	Si III	4,500	1.3	...	1
2796 ...	Mg II *k*	490,000	140	0.6	1

[a]Solar values from Rottman 1981, except for Mg II and soft X-ray where mean solar values from Ayres, Marstad, and Linsky 1981 were used.

[b]REFERENCES.—(1) This work; (2) Ayres, Marstad, and Linsky 1981.

atmosphere. Since hydrogen is the dominant constituent of the atmosphere, this process can be unstable; care must therefore be taken to ensure consistency between the RT and SE equations before integrating the hydrostatic equilibrium equation. Our computer code uses a complete linearization scheme described by Auer and Heasley (1976), which is more economical in terms of computing time than the original formulation (Auer and Mihalas 1970; Auer 1973; Auer, Heasley, and Milkey 1972) when many frequency points are involved. Our hydrogen model atom consisted of the five lowest bound levels plus the continuum. We solved explicitly for the Lyman-continuum, Lyα, Lyβ, and Hα transitions. Other radiative transitions were included as fixed rates in the nonvarying part of the rate matrix. These fixed radiative rates were expressed in terms of a radiation temperature (e.g., Auer *et al.*), and were calculated with a simple absorption and scattering source function in order to evaluate the radiation fields in a number of continua and subordinate transitions. For Lyα, Lyβ, and Hα, we used Voigt profiles and also included a schematic Stark broadening treatment for Hα. Since these lines were

computed with the complete redistribution (CRD) formulation, which is a poor assumption for very optically thick resonance lines, we approximated the effects of a more realistic redistribution function by including only the innermost six Doppler widths for Lyα and Lyβ (cf. Milkey and Mihalas 1973). The collisional excitation and ionization cross section were adopted from Sampson and Golden (1970), Golden and Sampson (1971), and Mihalas (1967). Upon convergence, we then had a self-consistent model available to be used as input in the subsequent Mg and C calculations.

3. We next solved the RT and SE equations for Mg II assuming CRD and using essentially the same computer code as in the previous step. The Mg model atom used is described in Table 3, the explicitly treated transitions in Table 4, and the adopted radiation temperatures in Table 5. Collisional excitation and ionization cross sections were taken from Shine (1973). After reaching a converged CRD solution, the Mg II populations and parameters for the equivalent two-level atom consisting of the lower and upper levels for the k line were stored and used as input for the next program.

4. The data stored by the CRD Mg II program were then used as input by a Mg II PRD program that assumes an equivalent two-level atom approach (Mihalas *et al.* 1976). For these calculations we did not utilize the capability of the code to include systematic velocity fields since the observed Mg II resonance lines are nearly symmetric.

5. We next solved the RT and SE equations for C II in a way similar to that described in step (3), except that

TABLE 3

MODEL ATOMS

Level No.	Level Designation	g_J	E[a] (cm^{-1})
	Mg II CRD		
1	Mg I $3s^2\,{}^1S$	1.	0.
2	Mg II $3s\,{}^2S$	2.	61669.(0.)
3	$3p\,{}^2P^o$	2.	35669.
4	$3p\,{}^2P^o$	4.	35761.
5	$3d\,{}^2D$	4.	71490.
6	$3d\,{}^2D$	6.	71491.
7	Mg III $2p^6\,{}^1S$	1.	121267.(0.)
	C II		
1	C I $2s^22p^2\,{}^3P$	9.	0.
2	C I $2s^22pnl$[a]	200.	88000.
3	C II $2s^22p\,{}^2P^o$	2.	90820.(0.)
4	$2s^22p\,{}^2P^o$	4.	63.
5	C I $2s2p^3\,{}^3S^o$	3.	105799.
6	C II $2s2p^2\,{}^4P$	2.	43003.
7	$2s2p^2\,{}^4P$	4.	43025.
8	$2s2p^2\,{}^4P$	6.	43054.
9	$2s2p^2\,{}^2D$	6.	74930.
10	$2s2p^2\,{}^2D$	4.	74933.
11	$2s2p^2\,{}^2S$	2.	96494.
12	$2s2p^2\,{}^2P$	2.	110624.
13	$2s2p^2\,{}^2P$	4.	110665.
14	$2s^2nl$[b]	100.	190000.
15	C III $2s^2\,{}^1S$	1.	196665.(0.)
	C III–IV		
1	C II $2s^22p\,{}^2P^o$	6.	0.
2	C III $2s^2\,{}^1S$	1.	196665.(0.)
3	$2s2p\,{}^3P^o$	1.	52367.
4	$2s2p\,{}^3P^o$	3.	52391.
5	$2s2p\,{}^3P^o$	5.	52447.
6	$2p^2\,{}^1P^o$	3.	102352.
7	$2p^2\,{}^3P$	1.	137426.
8	$2p^2\,{}^3P$	3.	137454.
9	$2p^2\,{}^3P$	5.	137502.
10	$2p^2\,{}^1D$	5.	145876.
11	$2p^2\,{}^1S$	1.	182520.
12	$2s\,nl$[b]	200.	350000.
13	C IV $2s\,{}^2S$	2.	386241.(0.)
14	$2p\,{}^2P^o$	2.	64484.
15	$2p\,{}^2P^o$	4.	64592.
16	nl[b]	200.	480000.
17	C V $1s^2\,{}^1S$	1.	520178.(0.)

[a]Energies for excited levels are given relative to the ground state for that ion. Energies for the lowest level in each ion are given relative to the next lower ion.

[b]This level is a collection of levels close to the continuum to which electrons cascade from autoionizing states.

TABLE 4

TRANSITIONS SOLVED EXPLICITLY

From Level	To Level	λ (Å)	f	a_{ν_0} (cm^{-2})
	Mg II CRD			
1	2	...	...	1.20–18
2	3	2803.5	0.32	
2	4	2796.3	0.64	
3	5	2791.7	0.915	
4	6	2798.7	0.824	
	C II			
3	10	1334.5	0.111	
{4	10	1335.66	0.0115	
{4	9	1335.71	0.102	
3	11	1036.3	0.131	
4	11	1037.0	0.131	
	C III–IV			
2	6	977.0	0.73	
{4	8	1175.59	0.0711	
{5	9	1175.71	0.213	
4	9	1174.9	0.118	
3	8	1175.3	0.284	
4	7	1176.0	0.0947	
5	8	1176.4	0.0709	
13	15	1548.2	0.381	
13	14	1550.8	0.190	

NOTE.—The braces indicate transitions that are treated as blends.

TABLE 5

ADOPTED RADIATION TEMPERATURES FOR TRANSITIONS WITH FIXED RATES

From Level	To Level	T_{rad} (K)	Type[a]
H			
2	6[b]	4500	P
3	6[b]	3900	P
4	6[b]	3775	P
5	6[b]	3525	P
1	4	6050	C
1	5	6150	C
2	4	4350	P
2	5	4400	P
3	4	3625	P
3	5	3825	P
4	5	3150	P
Mg II			
2	7[b]	6680	C
3, 4	7[b]	5460	C
5, 6	7[b]	4340	P
C II			
1	3[b]	5650	C
2	3[b]	3250	P
C II (*cont.*)			
3, 4	15[b]	9000	C
6, 7, 8 ...	15[b]	7730	C
9, 10	15[b]	6690	C
11	15[b]	5920	C
12, 13	15[b]	5500	C
14	15[b]	3750	P
C III–IV			
1	2[b]	9000	C
2	13[b]	13980	C
3, 4, 5 ...	13[b]	12650	C
6	13[b]	11360	C
7, 8, 9 ...	13[b]	10430	C
10	13[b]	10200	C
11	13[b]	9200	C
13	17[b]	17170	C
14, 15	17[b]	15670	C
2	12	13100	C
6	10	4400	P
6	11	5300	C
13	16	16300	C

[a] C and P indicate that the local electron temperatures are used to determine the radiative rates below this temperature (T_{rad}) in the chromosphere (C) or in the photosphere (P). Above this point T_{rad} is used to determine the rate.

[b] Continua.

we allowed for the depletion of C due to CO formation. More importantly since the λ1335 line is a close blend, we used a computer code that can handle blends. This code is described by Shine, Lites, and Chipman (1978), and we wish to thank Dr. B. Lites for allowing us to use a copy of this code. The C II model atom, transitions, and collisional rates are the same as used by Lites, Shine, and Chipman (1978) and are also given in Tables 3 and 4. The adopted radiation temperatures can be found in Table 5.

6. To calculate the C III and C IV emission lines, we used the same computer code as in step (5), with nearly

TABLE 6

MODEL PARAMETERS AND COMPUTED LINE SURFACE FLUXES

Model	m_{top} (g cm^{-2})	$\Delta \log m_R$ 22,500 K Plateau	ξ_t (km s^{-1})	Surface Flux (ergs cm^{-2} s^{-1}) C II 1334,5	C III 1176	C IV 1548,50	Mg II 2796
I	5.8(−8)	0.0	2–10	6950	3350	1600	190,000
IIa	5.8(−8)	0.0	2–10	5300	1600	400	(190,000)
IIb	2.0(−6)	0.0	2–10	...	3350	2600	(190,000)
IIIa	3.0(−6)	0.0	2–10	2200	2050	3100	180,000
IIIb	4.5(−6)	0.0	v_{sound}	2000	2250	3500	(180,000)
IVa	3.0(−6)	0.15	2–10	4100	(2050)	(3100)	(180,000)
IVb	4.5(−6)	0.15	v_{sound}	3350	(2250)	(3500)	(180,000)
V	4.5(−6)	0.15	v_{sound}	(3350)	(2250)	(3500)	420,000
Observed flux ...	...	...	...	3500	2900	3600	490,000

NOTE.—Surface fluxes in parentheses were not explicitly computed for the model, but assumed equal to the fluxes computed from a model with the same $T(m_R)$ structure in the region of line formation.

the same model atom as used by Lites and Cook (1979). See Tables 3, 4, and 5 for the relevant parameters.

IV. RESULTS AND DISCUSSION

a) The Chromosphere and Transition Region

In the process of arriving at our final model, we computed line profiles and fluxes for a number of models differing in assumed values of m_{top}, $T(m_R)$, and turbulent velocities, $v_t(m_R)$. A full chronological account of these different test models would not be informative, but we will describe some of the important criteria that led us to the final model. The parameters and computed line surface fluxes for each model are summarized in Table 6. Temperature distributions, $T(m_R)$, for each of the five models (designated by roman numerals) are shown in Figure 3. We assumed two different turbulent velocity distributions (see Fig. 3): a distribution in which $v_t(m_R)$ increases from 2 to 10 km s^{-1} and a distribution in which $v_t(m_R)$ equals the local sound speed.

We first determined a good value for the top mass, $m_{top} = 4.5 \times 10^{-6}$ g cm^{-2}, corresponding to $P_{top} = 0.0036$ dyn cm^{-2}, by finding an atmospheric model that predicts the surface flux in the C IV 1548, 1551 Å doublet in good agreement with the observed value. In this model, Model III, and in Models IV and V which are essentially identical in the TR, optical depth unity at line center in the 1548 Å line occurs at 72,000 K and the line center total optical depth in the TR is 4.8.

Unfortunately, the calculated flux for the C II 1334, 5 Å doublet turned out to be only one-half the observed value (see Table 6). Conceivably, this low value for the C II flux could be due to an error in the adopted value of T_{rad} for the ground state of C II. Since the threshold is located at 508 Å, photoionization in the He I continuum could be in error if the He–He$^+$ ionization is far out of equilibrium. This, however, is not the cause of the poor match to the observed C II flux, since trial calculations showed that a change in T_{rad} by 1000 K produced less than a 10% change in the C II flux. We then noted that the maximum in the contribution function for the C II 1334, 1335 Å lines occurs near 23,000 K. Therefore, to increase the flux in the C II lines while keeping the flux in the C IV lines unchanged, we introduced into Models IV and V a plateau at 22,500 K with a width of $\Delta \log m_R = 0.15$. Similar plateaus have been introduced into models for the Sun (e.g., Vernazza, Avrett, and Loeser 1981) and ε Eri (Simon, Kelch, and Linsky 1980). The corresponding changes in the C II flux were an increase from 2200 to 4100 ergs cm^{-2} s^{-1} for Model IVa (see below) and from 2000 to 3350 ergs cm^{-2} s^{-1} for Model V. These larger values of the surface flux are consistent with the observed flux of 3500 ergs cm^{-2} s^{-1}. Nevertheless, the derived temperature and width of the plateau should be viewed only as parametric description

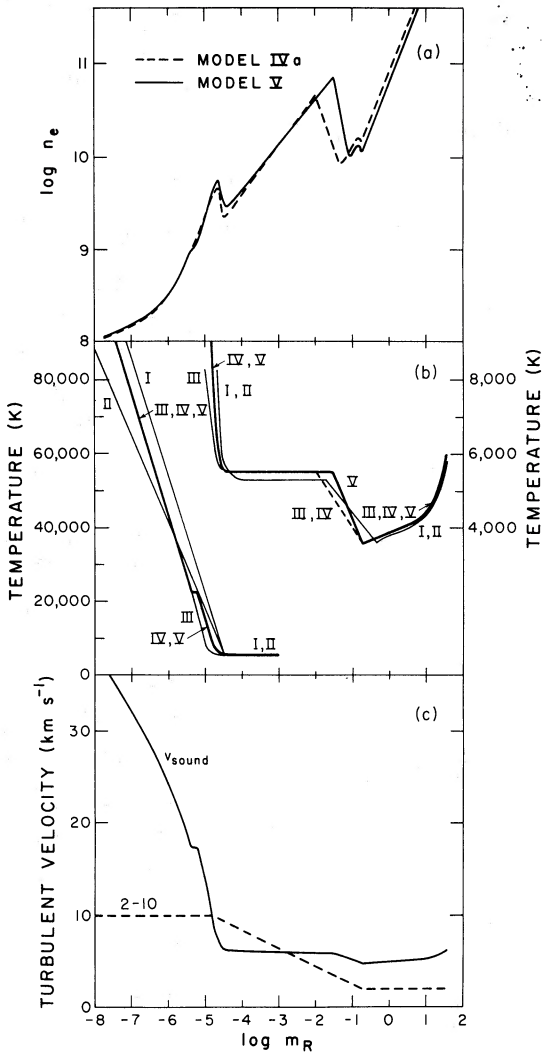

FIG. 3.—The electron density distributions (*top*), temperature distributions (*middle*), and turbulent velocity distributions (*bottom*) for the different models considered. The independent variable is the reduced column mass density, $m_R = m - m_{top}$, where m is the column mass density and $m_{top} = 4.5 \times 10^{-6}$ g cm^{-2} is the mass column above the top grid point in Model V at $T = 10^5$ K.

of the amount of material needed to produce the observed C II emission.

The temperature structure of the lower and middle chromosphere was determined by obtaining a good match between computed and observed Mg II k line profiles. The form of the $T(m_R)$ distribution we adopted in this region is a plateau at the temperature T_p, extending from $m_R = m_1$ to $m_R = m_2$ ($m_1 > m_2$). $T(m_R)$ is assumed linear in $\log m_R$ between m_1 and m_{min}. Above the point $m_R = m_2$, the $T(m_R)$ relation steepens smoothly to join the TR temperature rise beginning at $T = 8000$ K. We tried a number of models with differing values of T_p, m_1, and m_2 to obtain a good match

between the Mg II k line flux and profile. Several of these models are shown in Figure 3, and the computed Mg II fluxes are listed in Table 6. The model that best fits the Mg II k line flux is Model V with $T_p = 5500$ K, and we found that the Mg II k line flux is very sensitive to the values of T_p and m_1.

Two models, designated Models IVa and V, predict surface fluxes for the C II and C IV lines in good agreement with the observed values (see Table 6). The temperature distributions (see Fig. 3) in the upper chromosphere and TR are quite similar, but the turbulent velocity distributions, $v_t(m_R)$, are quite different. The model atmosphere for the preferred Model V, which provides the better fit to the Mg lines, is tabulated in Table 7. In Figure 4 we compare the observed and computed (PRD, Model V) profiles of the Mg II k line

TABLE 7

MODEL ATMOSPHERE FOR BETA CETI. MODEL V

m_R (g cm^{-2})	T (K)	n_e (cm^{-3})	ρ (g cm^{-3})	$v_{\rm turb}$ (km s^{-1})	H I		z (km)
					b_1	b_2	
1.88−8.....	100,000	1.14+8	2.24−16	36.7	2.76+9	1.78+2	1.264+5
5.00−8.....	86,000	1.33+8	2.63−16	34.0	2.28+9	1.72+2	1.251+5
1.34−7.....	71,860	1.62+8	3.20−16	31.1	1.80+9	1.76+2	1.222+5
2.59−7.....	62,430	1.92+8	3.79−16	29.0	1.48+9	1.96+2	1.186+5
5.00−7.....	53,000	2.38+8	4.68−16	26.7	1.15+9	2.57+2	1.129+5
7.75−7.....	46,510	2.86+8	5.63−16	25.0	9.22+8	3.68+2	1.076+5
1.20−6.....	40,170	3.57+8	7.05−16	23.2	7.01+8	6.44+2	1.008+5
1.86−6.....	34,140	4.69+8	9.26−16	21.4	4.92+8	1.36+3	9.268+4
2.59−6.....	29,430	6.06+8	1.20−15	19.9	3.33+8	2.59+3	8.582+4
4.02−6.....	22,750	9.36+8	1.87−15	17.4	1.16+8	5.37+3	7.638+4
5.00−6.....	22,500	1.06+9	2.11−15	17.3	9.65+7	5.75+3	7.144+4
5.95−6.....	22,500	1.16+9	2.33−15	17.3	8.88+7	5.79+3	6.716+4
7.09−6.....	20,000	1.40+9	3.01−15	16.0	4.27+7	5.58+3	6.290+4
8.44−6.....	17,500	1.75+9	3.90−15	14.9	1.54+7	4.34+3	5.899+4
1.00−5.....	15,000	2.26+9	5.20−15	13.7	3.93+6	2.63+3	5.546+4
1.20−5.....	12,500	2.96+9	7.30−15	12.3	6.06+5	1.17+3	5.240+4
1.42−5.....	10,000	3.64+9	1.16−14	10.4	3.43+4	3.87+2	4.991+4
1.55−5.....	8,750	4.10+9	1.50−14	9.45	3.87+3	1.97+2	4.893+4
1.68−5.....	7,800	4.54+9	1.86−14	8.74	4.41+2	1.05+2	4.817+4
1.87−5.....	7,000	5.03+9	2.35−14	8.10	4.47+1	5.41+1	4.728+4
2.10−5.....	6,500	5.46+9	2.90−14	7.66	8.27	3.29+1	4.639+4
2.35−5.....	6,000	5.52+9	3.67−14	7.14	1.40	1.84+1	4.561+4
2.86−5.....	5,600	3.74+9	5.34−14	6.44	0.79	1.08+1	4.446+4
3.82−5.....	5,500	2.96+9	7.42−14	6.20	1.11	9.33	4.297+4
6.18−5.....	5,500	3.54+9	1.18−13	6.13	1.26	9.26	4.047+4
1.00−4.....	5,500	4.50+9	1.88−13	6.10	1.27	9.21	3.793+4
1.59−4.....	5,500	5.65+9	2.96−13	6.07	1.29	9.14	3.551+4
2.51−4.....	5,500	7.08+9	4.67−13	6.04	1.31	9.04	3.308+4
3.98−4.....	5,500	8.87+9	7.41−13	6.02	1.34	8.91	3.065+4
6.31−4.....	5,500	1.11+10	1.18−12	6.00	1.38	8.74	2.822+4
1.00−3.....	5,500	1.38+10	1.87−12	5.99	1.42	8.54	2.579+4
1.59−3.....	5,500	1.72+10	2.96−12	5.98	1.47	8.31	2.337+4
2.51−3.....	5,500	2.14+10	4.70−12	5.97	1.52	8.08	2.095+4
3.98−3.....	5,500	2.67+10	7.47−12	5.97	1.57	7.85	1.854+4
6.31−3.....	5,500	3.34+10	1.19−11	5.96	1.61	7.65	1.612+4
1.00−2.....	5,500	4.18+10	1.88−11	5.96	1.64	7.47	1.372+4
1.52−2.....	5,500	5.15+10	2.85−11	5.96	1.67	7.35	1.151+4
2.30−2.....	5,500	6.36+10	4.33−11	5.95	1.68	7.28	9.300+3
3.49−2.....	5,340	5.41+10	6.78−11	5.86	1.54	5.83	7.112+3
5.30−2.....	4,900	2.21+10	1.12−10	5.61	1.20	2.88	5.068+3
8.04−2.....	4,460	1.10+10	1.87−10	5.35	0.92	1.20	3.202+3
1.22−1.....	4,015	1.26+10	3.15−10	5.08	0.68	0.42	1.513+3
1.85−1.....	3,575	1.18+10	5.37−10	4.79	0.46	0.11	0.0
4.39−1.....	3,725	2.86+10	1.22−9	4.89	0.54	0.18	−2.996+3
1.04+0.....	3,875	6.83+10	2.79−9	4.99	0.64	0.28	−6.115+3
3.80+0.....	4,100	2.44+11	9.62−9	5.13	0.75	0.48	−1.102+4
1.21+1.....	4,545	9.18+11	2.77−8	5.40	1.01	1.01	−1.575+4
1.86+1.....	4,900	1.61+12	3.94−8	5.61	1.01	1.02	−1.769+4
2.49+1.....	5,275	2.77+12	4.89−8	5.82	1.01	1.01	−1.910+4
3.11+1.....	5,685	6.16+12	5.67−8	6.04	1.01	1.01	−2.027+4
3.47+1.....	5,990	1.17+13	6.01−8	6.20	1.00	1.00	−2.089+4

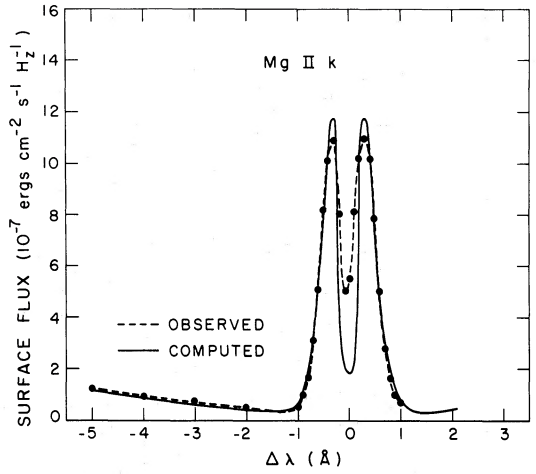

FIG. 4.—Comparison between the observed Mg II *k* line (2796 Å) profile and the computed profile for Model V.

(2796 Å), which are in excellent agreement except at line center. Here such comparisons inevitably fail, presumably because of the presence of velocity fields that cannot be described by Gaussian macroturbulence. To illustrate the formation of this line in PRD, we show in Figure 5 the monochromatic source functions for five wavelength positions in the line profile, and also where the monochromatic optical depths equal 0.67 at those wavelengths. Note that the integrated flux in the Mg II *k* line is very sensitive to the location in m_R of the onset of the 5500 K plateau (compare Model V with the other models in Fig. 3 and Table 6).

In Figure 6 we plot profiles of the C II 1334, 1335 Å lines and the C IV 1548, 1551 Å lines for Models IVa and V. The full profile is plotted for C II λ1335, but only half the profiles are plotted for the remaining lines, which are symmetric. These profiles can be compared with a 795 minute high-dispersion spectrum of β Ceti (image SWP 14786), which was obtained on 1981 August 19–20 by O. Engvold, E. Jensen, O. K. Moe, R. E. Stencel, and J. L. Linsky. Although this spectrum will be analyzed in a subsequent publication, it is important to mention here that the observed FWHM of the C IV λ1548 line is 0.33 Å. If we convolve an instrumental profile of 0.155 Å FWHM (30 km s^{-1}) with the computed profiles in Figure 6, the resulting FWHMs are 0.28 Å (Model IVa) and 0.41 Å (Model V). These comparisons suggest that the TR turbulent velocity distribution lies somewhere between 10 km s^{-1} and $v_t(m_R) = v_{\rm sound}(m_R)$. The close agreement of the observed and theoretical C IV and Mg II line widths as well as the Mg II, C II, C III, and C IV line fluxes argues that Model V is a near optimal fit to the ultraviolet data if our assumptions of a homogeneous plane-parallel atmosphere in hydrostatic equilibrium are valid.

b) Comparison of Chromosphere and Transition Region Parameters with Models of Other Stars

Since β Ceti lies very close to the TR dividing line and is the coolest star for which a TR model has now been computed, it is important to compare its model parameters with those derived for other stars. We list in Table 8 the mass column densities and pressures at the 8000 K level near the top of the chromosphere and at the 10^5 K level in the TR for the stars analyzed to date. Since the spectral features and computing codes used in analyzing these stars are similar but not identical, we searched for trends in these parameters rather than

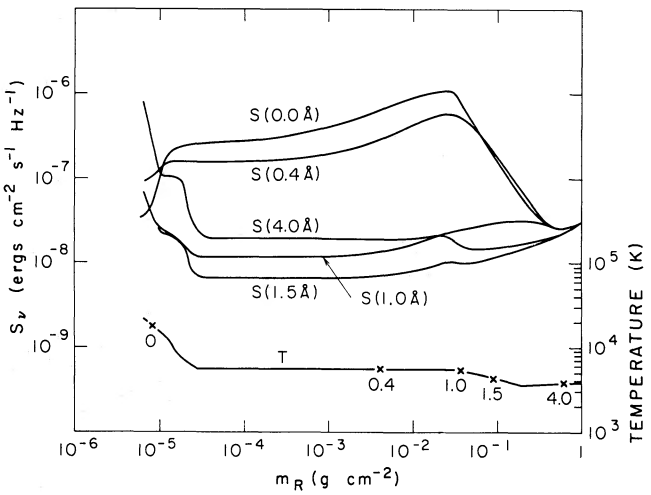

FIG. 5.—Monochromatic source functions for the Mg II *k* line at 0.0, 0.4, 1.0, 1.5, and 4.0 Å from line center. Also plotted are the temperature and location of monochromatic optical depth unity for each wavelength in the line (noted by the cross symbols on the temperature curve). Note that the source functions at 0.0 and 0.4 Å depend on m_R in a way similar to complete redistribution, and the source functions at larger wavelengths from line center depend on m_R in a way similar to coherent scattering.

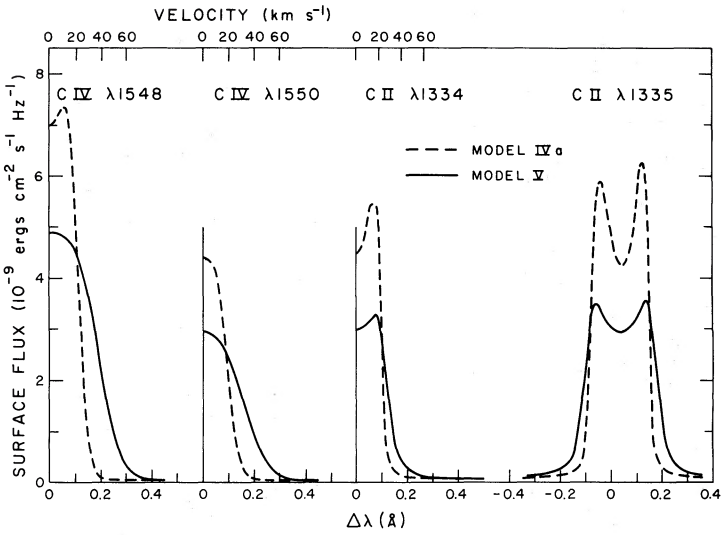

FIG. 6.—Computed C IV and C II profiles for Models IVa and V. The plotted half profiles are symmetric, but the full C II λ1335 profile is plotted because it is a close doublet.

TABLE 8

COMPARISON OF CHROMOSPHERE AND TRANSITION REGION MODEL PARAMETERS

Star	Spectral Type	log g	$m_{8000\,K}$ (g cm^{-2})	$P_{8000\,K}$ (dyn cm^{-2})	$m_{10^5\,K}$ (g cm^{-2})	$P_{10^5\,K}$ (dyn cm^{-2})	References[a]
Dwarfs and Subgiants							
α CMi	F5 IV–V	4.0	1 (−5)	0.10	...	...	1
Quiet Sun	G2 V	4.44	5.6(−6)	0.16	5.4(−6)	0.15	2
α Cen A	G2 V	4.26	5 (−6)	0.09	...	...	2
HR 1099 / UX Ari	K0 IV	3.5	...	...	~1 (−4)	~0.4	3
α Cen B.....	K1 V	4.47	3 (−6)	0.10	...	...	2
ε Eri.....	K2 V	4.5	2 (−5)	0.6	1.6(−5)	0.5	4
EQ Vir	dK5	4.75	5 (−5)	2.8	...	...	5
GL 411	dM2	4.75	1 (−6)	0.06	...	...	5
Giants							
Capella Ab ...	F9 III	3.1	~2 (−4)	~0.3	~3 (−4)	~0.4	6
β Cet	G9.5 III	2.9	2.1(−5)	0.017	4.5(−6)	0.0036	7
β Gem.....	K0 III	2.9	1.6(−5)	0.016	...	...	8
α Boo	K1+ IIIb	1.7	3.2(−5)	0.0016	...	...	9
α Tau	K5 III	1.4	1.4(−4)	0.0035	...	...	8
Bright Giants and Supergiants							
β Dra	G2 Ib–II	1.35	2.0(−3)	0.045	...	...	10
ε Gem	G8 Ib	0.85	<1 (−6)	<7 (−6)	...	...	10
α Ori	M2 Ia–Iab	0.0	<1 (−6)	<1 (−6)	...	...	10

[a]REFERENCES.—(1) Ayres, Linsky, and Shine 1974. (2) Ayres *et al.* 1976. (3) Simon and Linsky 1980. (4) Simon, Kelch, and Linsky 1980. (5) Giampapa, Worden, and Linsky 1982. (6) Ayres and Linsky 1980. (7) This paper. (8) Kelch *et al.* 1978. (9) Ayres and Linsky 1975. (10) Basri, Linsky, and Eriksson 1981.

small differences between the parameters for different stars. We believe that the following trends are likely to be real.

1. Pressures at the top of the chromosphere, $P_{8000\ K}$, for the two giant stars immediately to the left of the TR dividing line (β Ceti and β Gem) are an order of magnitude smaller than for quiet dwarfs (i.e., the quiet Sun, α Cen A, α CMi) and an order of magnitude larger than for the two giant stars lying immediately to the right of the TR dividing line (α Boo and α Tau). Since $P = nkT$, the densities at the top of the chromosphere similarly decrease one order of magnitude from the quiet dwarfs to the K0 III stars and another order of magnitude to the later K giants. The decrease in $P_{8000\ K}$ along this sequence is a result of gravity decreasing much faster than $m_{8000\ K}$ increases along the sequence. Despite these trends, $(f_{Mg\ II}/l_{bol})$ is similar in β Ceti and the quiet Sun (see Table 2), because the increased geometrical scale of the chromosphere in β Ceti compensates for the lower chromospheric densities.

2. We have far less information on TR pressures in stars, but $P_{10^5\ K}$ in β Ceti appears to be a factor of 50 smaller than in dwarf stars (quiet Sun, ε Eri) and the RS CVn type systems (HR 1099, UX Ari, Capella Ab). In fact, β Ceti has the lowest TR pressure yet determined for a star. This suggests that $P_{10^5\ K}$ decreases significantly as a single star evolves toward the TR boundary, presumably as a consequence of decreasing rotation and dynamo generation of magnetic fields. To the right of the boundary, either stars have no 10^5 K plasma or $P_{10^5\ K}$ is very much smaller than for β Ceti as implied by the small values of $P_{8000\ K}$ for α Boo, α Tau, ε Gem, and α Ori. Nevertheless, the value of $(f_{C\ IV}/l_{bol})$ for β Ceti is the same as for the quiet Sun. Since the strength of C IV emission is roughly proportional to $P^2_{10^5\ K}(dT/dh)^{-1}$, the factor of 50 decrease in $P_{10^5\ K}$ from the quiet Sun to β Ceti is compensated by a factor of 2500 increase in the geometrical scale of the β Ceti TR. This suggests that other giants and supergiants with TR emission lines probably have TRs that are similarly extended

c) *The Corona*

From the observed soft X-ray flux, $f_x = 2.0\times10^{-11}$ ergs cm^{-2} s^{-1} (AML), and distance of β Ceti, we infer a 0.2–4 keV X-ray luminosity of $L_x = 6.5\times10^{29}$ ergs s^{-1}. This is a rather large luminosity for a single G giant and is only a factor of 3 smaller than the L_x of Capella (α Aur). We calculate a volume emission measure (EM) from

$$L_x = \mathrm{EM}\int_{0.2}^{4\ \mathrm{keV}} P(E)\,dE,$$

where $P(E)$ is the power coefficient given by Raymond and Smith (1977). The integral in this expression was evaluated by writing $P(E) = a\cdot10^b$ and obtaining values of a and b from their graphs of $P(E)$ as a function of plasma temperature. The derived values of

$$\int_{0.2}^{4\ \mathrm{keV}} P(E)\,dE$$

are 4.5×10^{-24} for $T = 3\times10^6$ K and 6.4×10^{-24} for $T = 1\times10^7$ K. Thus EM $= 1.7\times10^{53}$ cm^{-3} for $T = 3\times10^6$ K and EM $= 1.2\times10^{53}$ cm^{-3} for $T = 1\times10^7$ K.

These derived emission measures can now be compared with some simple calculations for the corona of β Ceti. We first consider the simplest possible model: an isothermal homogeneous corona in hydrostatic equilibrium with a gas pressure scale height $H = 5.1\times10^{11}$ cm (0.8 $R_\star$) for $T = 3\times10^6$ K or $H = 17.1\times10^{11}$ cm (2.8 $R_\star$) for $T = 10^7$ K. Since the corona is extended,

$$\mathrm{EM} = \int_{h_0}^{\infty} n_e^2\,dV = 4\pi n_{e0}^2\left(\frac{Hh_0^2}{2} + \frac{H^2h_0}{2} + \frac{H^3}{4}\right), \quad (1)$$

where $h_0 = 1.3\times10^{10}$ cm is the height of the base of the corona (see Table 7). For this model the derived gas pressure at the base of the corona is $P_g = 0.49$ dyn cm^{-2} for $T = 3\times10^6$ K or $P_g = 0.23$ dyn cm^{-2} for $T = 1\times10^7$ K, corresponding to a mass column density at the top of the TR of $m_{top} = 6.2\times10^{-4}$ g cm^{-2} for $T = 3\times10^6$ K or $m_{top} = 2.9\times10^{-4}$ g cm^{-2} for $T = 1\times10^7$ K. These values of m_{top} are 60–130 times larger than that previously derived from our analysis of the ultraviolet emission lines, primarily C IV. One possible way out of this inconsistency is to assume a geometry in which the magnetic field confines the TR plasma to only a portion of the stellar surface and then diverges at greater altitudes to fill the whole volume in the corona. From our C IV calculations, we have extrapolated what C IV surface flux would result from a 40-fold increase in m_{top} and derived an increase of a factor of 4, implying a TR filling factor of 25%. This value must be considered uncertain because of our extrapolation procedure.

Alternatively, we assume that, as on the Sun, the coronal X-ray emission is primarily from the hot plasma confined in a number of closed magnetic loops. If this plasma is static and the loop height L is smaller than the pressure scale height H, then the scaling law $T = 1400\,(PL)^{1/3}$, proposed by Rosner, Tucker, and Vaiana (1978), is valid. In Table 9 we list the parameters for such loops, assuming that the loops are cylinders with diameter $0.05L$ in the form of half-circles with footpoints perpendicular to the surface. Listed in Table 9 are the individual loop volume V_{loop}, pressure P_{loop}, electron density n_e, area projected onto the stellar surface A_{loop}, the number of loops N_{loop}, the fraction of the stellar disk covered by the loops f_{cover}, and the coronal mass column density at the base of the loops m_{cor}. The values of these parameters have been evaluated

TABLE 9

CORONAL LOOP PARAMETER

Parameter	$T = 3(6)$ K			$T = 1(7)$ K		
L (cm)	1 (10)	1 (11)	1 (12)	1 (10)	1 (11)	1 (12)
L/H	0.02	0.2	2.0	0.006	0.06	0.6
$V_{\rm loop} = 6.2(-3)\ L^3$ (cm^3)	6.2(27)	6.2(30)	6.2(33)	6.2 (27)	6.2 (30)	6.2 (33)
$P_{\rm loop} = 3.6(-10)\ T^3\ L^{-1}$ (dyn cm^{-2})	1.0	0.1	0.01	36	3.6	0.36
$n_e = 1.4(6)\ T^2\ L^{-1}$ (cm^{-3})	1.2 (9)	1.2 (8)	1.2(7)	1.4 (10)	1.4 (9)	1.4 (8)
$N_{\rm loop} = 8.5(-11)$ EM $T^{-4}\ L^{-1}$	1.8 (7)	1.8 (6)	1.8(5)	1.0 (5)	1.0 (4)	1.0 (3)
$A_{\rm loop} = 0.1\ L^2$ (cm^2)	1 (19)	1 (21)	1 (23)	1 (19)	1 (21)	1 (23)
$f_{\rm cover} = (N_{\rm loop} A_{\rm loop}/A_\star) 1.8(-36)$ EM $T^{-4}\ L$	37	370	3700	0.2	2	20
$m_{\rm cor} = 4.5(-13)\ T^3 L^{-1}$ (g cm^{-2})	1.2(−3)	1.2(−4)	1.2(−5)	4.5 (−2)	4.5 (−3)	4.5(−4)

for two assumed coronal temperatures (3×10^6, 1×10^7 K) and for loop heights $L = 1\times10^{10}$ to 1×10^{12} cm, corresponding to 0.016–1.6 $R_\star$. Except for the $T = 3\times10^6$ K and $L = 10^{12}$ cm example, all of the cases considered are consistent with the $L/H < 1$ assumption of the model.

Given the model assumptions, we find no acceptable solutions for $T = 3\times10^6$ K because $f_{\rm cover} \gg 1$, but the solutions for $T = 1\times10^7$ K and $L \leq 1\times10^{11}$ cm are acceptable on this basis. The specific case of $T = 1\times10^7$ K and $L = 1\times10^{11}$ cm probably corresponds to loops totally covering the stellar surface, since toward the limb loops will overlie one another. The constraint that $f_{\rm cover} \lesssim 2$ results in a hot corona ($T \gtrsim 6\times10^6$ K), consisting of a large number of loops ($N_{\rm loop} > 10^4$) with high gas pressures ($P_{\rm loop} > 3.6$ dyn cm^{-2}) and base mass column densities ($m_{\rm cor} > 4.5\times10^{-3}$ g cm^{-2}), which are a factor of 10^3 larger than at the top of the TR.

These sample calculations demonstrate the difficult problem posed by stellar spectra in the absence of any information on the geometry, which could be highly inhomogeneous and controlled by closed magnetic loop structures as on the Sun. Although we are able to explain the Mg II, C II, and C IV lines formed over a wide range of temperature (5×10^3 to 1×10^5 K) by a one-component TR model in hydrostatic equilibrium, the X-ray data imply either that the TR is inhomogeneous or that the corona consists of loops with gas pressures a factor of 10^3 larger than at the top of the TR. This pressure imbalance is a common phenomenon, however, as it is present in solar active region loops (e.g., Rosner, Tucker, and Vaiana 1978) and in RS CVn systems (Walter *et al.* 1980; Swank *et al.* 1981). Therefore, we should probably not attempt to impose pressure balance between the TR and corona, but rather assume that magnetic forces in the coronal loops produce total (gas and magnetic) pressure balance and a resultant quasi-steady state environment. We encourage further studies of this important question.

V. CONCLUSIONS

We began this study by calling attention to the important location of β Ceti immediately to the left of the TR boundary in the H-R diagram. To investigate how the properties of stellar chromospheres and TRs change as a single star evolves toward this boundary, we computed a model to match the observed emission line fluxes and line profiles, and compared this model to models computed for stars located elsewhere in the H-R diagram. Our model for β Ceti, as well as the models for other stars to which it is compared, assumes horizontal homogeneity, hydrostatic equilibrium, and steady state conditions. We derived its $T(m)$ structure from the temperature minimum to 10^5 K in the TR so as to be consistent with the profiles of the Mg II k (PRD) and C IV λ1548 lines, as well as the integrated fluxes of the Mg II, C II, and C IV lines observed by *IUE*. Given the assumptions, we obtained a good match to these data.

Comparing the β Ceti model to models of other stars computed in a similar way, we found two interesting trends. First, pressures and therefore densities near the top of the chromosphere decrease an order of magnitude from the quiet dwarfs to the giants immediately to the left of the TR dividing line (β Ceti and β Gem), and decrease another order of magnitude to the giants immediately to the right of the TR dividing line (α Boo and α Tau). This trend is primarily due to decreasing gravity along this sequence. Despite this trend, the normalized Mg II flux for β Ceti is similar to that of the Sun, because of the increased geometrical scale of the β Ceti chromosphere. Stencel *et al.* (1981) have shown that the chromospheric densities in giants to the right of the TR boundary are so low that these chromospheres must extend several stellar radii. Thus the geometric scale of chromospheres increases rapidly as single stars evolve across the boundary.

Second, we found that the TR gas pressure, $P_{10^5\,\rm K}$, for β Ceti is very much lower than for any star previously studied. This suggests that as a single star evolves from the main sequence into the giant branch and then from left to right across the TR boundary, first the TR pressures decrease by roughly two orders of magnitude, and then as a star crosses the boundary the amount of 10^5 K gas becomes negligible. The basic cause underlying this change is likely to be decreasing stellar rotation and dynamo generation of magnetic fields as discussed

by Ayres, Simon, and Linsky (1982). It is interesting that despite the factor of 50 decrease in $P_{10^5\,K}$ between the Sun and β Ceti, the normalized C IV flux in these two stars is about the same, implying an increase in the geometrical scale by a factor of 2500 between the Sun and the β Ceti.

Finally, we discussed the corona of β Ceti based on the observed X-ray flux. We found that if the corona is homogeneous and isothermal then its pressure is about 100 times that of the TR it overlies. If, on the other hand, we assume that the hot coronal plasma is confined by static loops, then the corona must be hot ($T > 6 \times 10^6$ K) and the gas pressure in the loops a factor of 1000 times larger than the underlying TR. We therefore concluded that the corona and TR are probably both inhomogeneous, and that further work is needed to study how magnetic forces in the loops produce total (gas and magnetic) pressure balance in the TR and corona, and result in a quasi–steady state environment. In a subsequent paper we will analyze the high-dispersion *IUE* spectra and consider a two-component (loop and nonloop) atmospheric model for this star.

We wish to thank Drs. Kondo and Boggess, and the staff of the *IUE* Observatory, for their help in the acquisition of the spectra presented in this paper, and Dr. A. Brown for fitting the C IV line profile. We also wish to thank the National Center for Atmospheric Research, under contract with the National Science Foundation, for a generous allocation of CRAY-1 computer time. K.E. gratefully acknowledges the cooperation, support, and interest shown by the staffs and visitors at JILA and NCAR during his stay in Boulder. This work was supported by grants NGL-06-003-057 and NAG5-82 from the National Aeronautics and Space Administration to the University of Colorado, which we gratefully acknowledge.

REFERENCES

Auer, L. H. 1973, *Ap. J.*, **180**, 469.
Auer, L. H., and Heasley, J. N. 1976, *Ap. J.*, **205**, 165.
Auer, L. H., Heasley, J. N., and Milkey, R. W. 1972, KPNO Contr. No. 555.
Auer, L. H., and Mihalas, D. 1970, *M.N.R.A.S.*, **149**, 65.
Ayres, T. R. 1979, *Ap. J.*, **228**, 509.
Ayres, T. R., and Linsky, J. L. 1975, *Ap. J.*, **200**, 660.
_____. 1980, *Ap. J.*, **241**, 279.
Ayres, T. R., Linsky, J. L., Rodgers, A. W., and Kurucz, R. L. 1976, *Ap. J.*, **210**, 199.
Ayres, T. R., Linsky, J. L., and Shine, R. A. 1974, *Ap. J.*, **192**, 93.
Ayres, T. R., Linsky, J. L., Vaiana, G. S., Golub, L., and Rosner, R. 1981, *Ap. J.*, **250**, 293.
Ayres, T. R., Marstad, N. C., and Linsky, J. L. 1981, *Ap. J.*, **247**, 545 (AML).
Ayres, T. R., Simon, T., and Linsky, J. L. 1982, *Ap. J.*, **263**, 791.
Basri, G. S., Linsky, J. L., and Eriksson, K. 1981, *Ap. J.*, **251**, 162.
Bell, R. A., Eriksson, K., Gustafsson, B., and Nordlund, A. 1976, *Astr. Ap. Suppl.*, **23**, 37.
Bell, R. A., and Gustafsson, B. 1978, *Astr. Ap. Suppl.*, **34**, 229.
Bernat, A. P., Honeycutt, R. K., Kephart, J. E., Gow, C. E., Sanford, M. T., II, and Lambert, D. L. 1978, *Ap. J.*, **219**, 532.
Cassatella, A., Holm, A., Ponz, D., and Schiffer, F. H. 1980, NASA *IUE* Newsletter, No. 8, p. 1 (also in ESA *IUE* Newsletter No. 5, p. 5).
Eggen, O. J. 1956, *A.J.*, **61**, 361.
Golden, L. B., and Sampson, D. H. 1971, *Ap. J.*, **163**, 405.
Giampapa, M. S., Worden, S. P., and Linsky, J. L. 1982, *Ap. J.*, **258**, 740.
Gray, D. F. 1982*a*, *Ap. J.*, **262**, 682.
_____. 1982*b*, private communication.
Hansen, L., and Kjaergaard, P. 1971, *Astr. Ap.*, **15**, 123.
Helfer, H. L. 1969, *A.J.*, **74**, 1155.
Hoffleit, D. 1982, *The Bright Star Catalog* (4th Rev. ed.; New Haven: Yale University Press).
Holm, A. 1979, NASA *IUE* Newsletter, No. 7, p. 27.
Iben, I., Jr. 1967, *Ap. J.*, **147**, 650.
Johnson, H. L., Mitchell, R. I., Iriarte, B., and Wisniewski, W. Z. 1966, *Comm. Lunar Planet. Lab.*, **4**, 99.
Keenan, P. C. 1982, private communication.
Kelch, W. L., Linsky, J. L., Basri, G. S., Chiu, H.-Y. Chang, S. H., Maran, S. P., and Furenlid, I. 1978, *Ap. J.*, **220**, 962.
Linsky, J. L. 1980, *Ann. Rev. Astr. Ap.*, **18**, 439.
Linsky, J. L., and Haisch, B. M. 1979, *Ap. J.* (*Letters*), **229**, L27.
Linsky, J. L., Worden, S. P., McClintock, W., and Robertson, R. M. 1979, *Ap. J. Suppl.*, **41**, 47.
Lites, B. W., and Cook, J. W. 1979, *Ap. J.*, **228**, 598.
Lites, B. W., Shine, R. A., and Chipman, E. G. 1978, *Ap. J.*, **222**, 333.
Mihalas, D. 1967, *Ap. J.*, **149**, 169.
Mihalas, D., Shine, R. A., Kunasz, P. B., and Hummer, D. G. 1976, *Ap. J.*, **205**, 492.
Milkey, R. W., and Mihalas, D. 1973, *Ap. J.*, **185**, 709.
O'Brien, G. T. 1980, Ph.D. thesis, University of Texas at Austin.
Pallavicini, R., Golub, L., Rosner, R., Vaiana, G. S., Ayres, T., and Linsky, J. L. 1981, *Ap. J.*, **248**, 279.
Raymond, J. C., and Smith, B. W. 1977, *Ap. J. Suppl.*, **35**, 419.
Rosner, R., Tucker, W. H., and Vaiana, G. S. 1978, *Ap. J.*, **220**, 643.
Rottman, G. J. 1981, *J. Geophys. Res.*, **86**, 6697.
Sampson, D. H., and Golden, L. B. 1970, *Ap. J.*, **161**, 321.
Shine, R. A. 1973, Ph.D. thesis, University of Colorado.
Shine, R. A., Lites, B. W., and Chipman, E. G. 1978, *Ap. J.*, **224**, 247.
Simon, T., Kelch, W. L., and Linsky, J. L. 1980, *Ap. J.*, **237**, 72.
Simon, T., and Linsky, J. L. 1980, *Ap. J.*, **241**, 759.
Simon, T., Linsky, J. L., and Stencel, R. E. 1982, *Ap. J.*, **257**, 225.
Smith, M. A., and Dominy, J. F. 1979, *Ap. J.*, **231**, 477.
Stein, R. F. 1981, *Ap. J.*, **246**, 966.
Stencel, R. E. 1978, *Ap. J.* (*Letters*), **223**, L37.
Stencel, R. E., Linsky, J. L., Brown, A., Jordan, C., Carpenter, K. G., Wing, R. F., and Czyzak, S. 1981, *M.N.R.A.S.*, **196**, 47P.
Stencel, R. E., and Mullan, D. J. 1980*a*, *Ap. J.*, **238**, 221.
_____. 1980*b*, *Ap. J.*, **240**, 718.
Swank, J. H., White, N. E., Holt, S. S., and Becker, R. H. 1981, *Ap. J.*, **246**, 208.
Ulmschneider, P. 1979, *Space Sci. Rev.*, **24**, 71.
Vernazza, J. E., Avrett, E. H., and Loeser, R. 1981, *Ap. J. Suppl.*, **45**, 635.
Walter, F. M., Cash, W., Charles, P. A., and Bowyer, C. S. 1980, *Ap. J.*, **236**, 212.
Woods, M. L. 1956, *Mem. Commonwealth Obs.*, **3**, 12.
Zirin, H. 1976, *Ap. J.*, **208**, 414.

KJELL ERIKSSON: Astronomiska Observatoriet, Box 515, 75120 Uppsala, Sweden

JEFFREY L. LINSKY: Joint Institute for Laboratory Astrophysics, University of Colorado, Boulder, CO 80309

THEODORE SIMON: Institute for Astronomy, University of Hawaii, 2680 Woodlawn Dr., Honolulu, HI 96821